Journal of Magnetism and Magnetic Materials 496 (2020) 165951

Contents lists available at ScienceDirect

Journal of Magnetism and Magnetic Materials

journal homepage: www.elsevier.com/locate/jmmm

Research articles

Influence of copper addition and heat treatment parameters on nanocrystallization process of Fe-Co-Mo-B-Si amorphous ribbons with high saturation magnetization about 1.6 T

Adrian Radoń[a,*], Rafał Babilas[b], Patryk Włodarczyk[a], Przemysław Zackiewicz[a], Dariusz Łukowiec[b], Marcin Polak[a], Mariola Kądziołka-Gaweł[c], Aleksandra Kolano-Burian[a], Łukasz Hawełek[a]

[a] Łukasiewicz Research Network – Institute of Non-Ferrous Metals, Sowinskiego 5 St., 44-100 Gliwice, Poland
[b] Faculty of Mechanical Engineering, Silesian University of Technology, Konarskiego 18 a St., 44-100 Gliwice, Poland
[c] Institute of Physics, University of Silesia, 75 Pułku Piechoty 1a St., 41-500 Chorzów, Poland

ARTICLE INFO

Keywords:
Nanocrystalline alloys
Amorphous structure
Crystallization kinetics
Fe alloys
High saturation magnetization

ABSTRACT

In this paper the influence of copper addition on the formation of the amorphous phase and the nanocrystallization process of $Fe_{79.8-x}Co_2Cu_xMo_{0.2}Si_4B_{14}$ (x = 0, 0.25, 0.5, 0.75, 1, 1.5, 2) ribbons was described. The formation of crystalline phases was described using differential scanning calorimetry, X-ray diffractometry, Mössbauer spectroscopy and transmission electron microscopy. It was confirmed that the addition of copper decreases the glass forming ability, while facilitating the process of nanocrystallization. The analysis of the Avrami exponent allowed to state, that for fully amorphous alloys the crystallization of the α-Fe phase is associated with diffusion-controlled growth with decreasing nucleation rate and the Fe_2B phase with interface controlled growth with increasing nucleation rate. Additionally, with increasing copper addition onset temperature of crystallization of α-Fe phase shifts to lower values, whereas for second, Fe_2B phase, these changes are not so visible. Optimization of the annealing process of toroidal cores made from amorphous ribbons with different copper content allowed to obtain nanocrystalline, soft magnetic materials characterized by low coercivity ~9 A/m and high saturation induction of about 1.6 T. Analysis of transmission electron microscope images and electron diffraction confirmed that high magnetic parameters are related to the coexistence of the amorphous and nanocrystalline phases, which was confirmed also by Mössbauer spectroscopy.

1. Introduction

The Fe-based amorphous and nanocrystalline alloys can be used in the various forms as magnetic cores and sensors, which is related to their high magnetic permeability (μ), low coercivity (H_c) and low power losses (P_s) [1–3]. The nanocrystallization process of amorphous alloys allows obtaining materials with lower coercivity and higher saturation magnetization than amorphous precursors [4]. These magnetic parameters can be easily modified by changing the heat treatment parameters such as temperatures, time and heating rate [5,6]. The optimal parameters of annealing of amorphous alloys can be determined on the basis of differential scanning calorimetry (DSC) curves through determination of onset temperatures of the first peak crystallization. Generally, this peak is associated with crystallization of α-Fe phase, whereas second peak with crystallization of for example Fe_2B phase. Therefore to avoid the precipitation of the second phase the increase of temperature difference between these peaks should be maximized. The presence and crystallization of FeB, Fe_2B and FeP phases is associated with addition of metalloids, which improve glass forming ability (GFA) of Fe-based alloys. However, the addition of these elements has negative impact on the preparing of nanocrystalline soft magnetic alloys with high saturation induction [1,7,8]. Therefore other chemical elements such as Cu are necessary to avoid precipitation of these phases, which is related to the shift of the first peak to lower temperatures. Interestingly, also addition other chemical elements such as Al and Nb can inhibit the precipitation of the second phase, which was discussed previously [9–11]. The Cu addition causes the phase segregation and formation of its clusters in amorphous matrix. These clusters are responsible for heterogenous crystallization of α-Fe phase [12]. Cu clusters grow diffuse and their positive impact on the formation of soft

* Corresponding author.
E-mail address: adrianr@imn.gliwice.pl (A. Radoń).

https://doi.org/10.1016/j.jmmm.2019.165951
Received 14 June 2019; Received in revised form 5 September 2019; Accepted 4 October 2019
Available online 08 October 2019

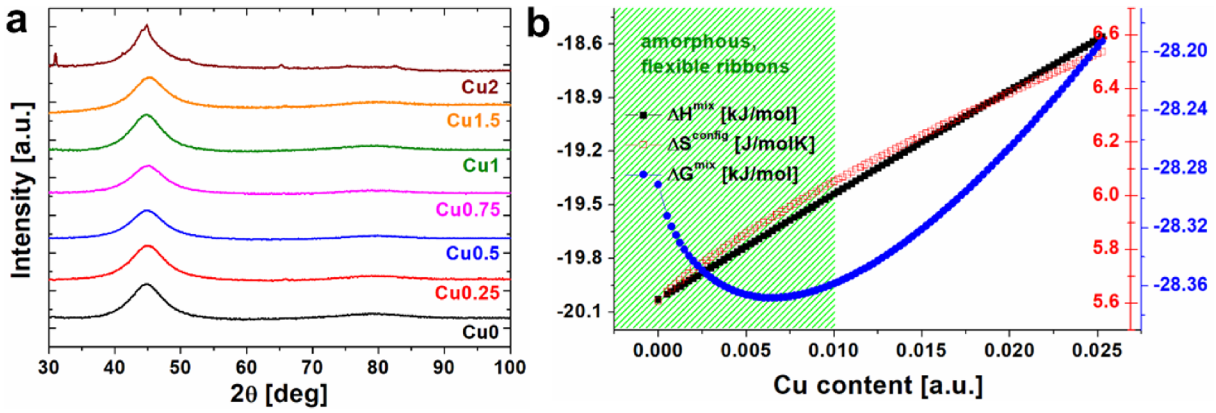

Fig. 1. a) XRD patterns of as-spun ribbons with different Cu content; b) thermodynamic parameters: ΔH^{mix}, ΔS^{config} and ΔG^{mix} in function of Cu content with marked region of fully amorphous and flexible ribbons state.

magnetic phase was confirmed for many different alloys such as Fe-Cu-Nb-Si-B and Fe-Zr-B-Cu alloys [13–16]. The Cu clusters have a short-range ordering with *fcc* structure and are formed on the early stage of annealing. Under continuous annealing, Fe atoms form nucleus and then crystallize into α-Fe phase on the Cu clusters-amorphous phase boundary [17].

According to the Random Anisotropy Model (RAM), the decrease of the grain size, below exchange length, can improve the magnetic properties of alloys. Generally, for Fe-based alloys minimum value of the exchange length is equal to 20–40 nm, therefore the nanocrystalline alloys with 5–20 nm grains are magnetically soft [18]. Additionally, not only grain size, but also their distribution affects on the magnetic properties. For example, nonhomogeneous and large grains increase the coercivity. Therefore to control growth of the grains many different alloying additives are used. It means, that the chemical composition of alloys determine not only glass forming ability but also parameters of heat treatment and consequently magnetic properties. Lashgari et al. described the influence of addition of different chemical elements on the formation of amorphous and nanocrystalline phases in Fe-based alloys [19]. They concluded, that the silicon and boron improve GFA, however addition of B above 10% at. has a negative impact on the magnetic properties. Moreover, the controlled Cu addition has a positive impact on the crystallization of nanometric grains with uniform distribution.

The aim of this study was to describe the nanocrystallization process of $Fe_{79.8-x}Co_2Cu_xMo_{0.2}Si_4B_{14}$ amorphous alloys in form of the ribbons with different Cu content. The prepared ribbons were used to produced toroidal cores, which were annealed to obtain nanocrystalline cores with high saturation magnetization and low coercivity. The optimal parameters of heat treatment as well as their influence on the structure of alloys were determined. Therefore the presented alloys can be successfully applicated as the soft magnetic cores.

2. Materials and methods

The amorphous $Fe_{79.8-x}Co_2Cu_xMo_{0.2}Si_4B_{14}$ (x = 0, 0.25, 0.5, 0.75, 1, 1.5, 2) alloys in form of ribbons were prepared in double stage process. The samples were marked as Cu0, Cu0.25, Cu0.5, Cu0.75, Cu1, Cu1.5 and Cu2, respectively. Firstly, crystalline precursors were produced from pure chemical elements (Fe, Si, Mo, Cu and Co) and FeB_{18} alloy using induction furnace VIM-LAB 50-60. Afterwards, the crystalline precursors were remelted and melt-spun from liquid state (1473.15 K) at a copper wheel surface speed of 33 m/s. The verification of amorphous structure and its changes induced by isochronal and isothermal annealing were performed using X-ray diffractometer MiniFlex 600 with copper tube (Cu Kα, λ = 1.5406 Å) and strip detector D/teX Ultra. The crystallization process was described on the basis of DSC curves recorded using thermal analyzer Netzsch STA 449F3. To determine structure changes around the Fe atoms causes by heat the ^{57}Fe Mössbauer spectra were recorded at room temperature with a constant acceleration spectrometer equipped with ^{57}Co:Rh source (activity ~10 mCi), multichannel analyzer (1024 channels) and linear ^{57}Co source arrangement, absorber and detector. A metallic iron foil (α-Fe) absorber was used for velocity and isomer shift calibration of the Mössbauer spectrometer. Additionally, high resolution transmission electron microscopy (HRTEM) images and selected area electron diffraction (SAED) patterns were recorded for amorphous and annealed samples using S/TEM TITAN 80-300 electron microscope. The obtained images and diffraction patterns were then analyzed using CrystBox software (version 1.10 (build 0066), Institute of Physics of the Czech Academy of Sciences [20,21]). The magnetic measurements at ambient temperature were performed using Remacomp-C-1200 measuring system for samples in form of cores (weight about 20 g) produced from amorphous ribbons with width equal to 10 mm. The hysteresis loops recorded for frequency equal to 50 Hz and for applied field up to 1000 A/m.

3. Results and discussion

The amorphous state of melt spun ribbons was verified using XRD method. The recorded XRD patterns for all samples with 0–2 at. % of Cu are presented in Fig. 1a. The amorphous ribbons were obtained from alloys with Cu content lower than 2% at. Moreover, only ribbons with Cu up to 1% at. were flexible. To determine influence of copper content on the formation of amorphous phase three thermodynamic parameters: enthalpy of mixing (ΔH^{mix}), configurational entropy (ΔS^{config}) and Gibbs free energy of mixing (ΔG^{mix}) were calculated according to the Eqs. (1)–(3) for broad Cu range and presented in Fig. 1b. For the tested samples values of these parameters are presented also in Table 1.

Table 1
The values of thermodynamic parameters calculated for alloys in casting temperature (T = 1473.15 K).

Alloy	ΔH^{mix} [kJ/mol]	ΔS^{config} [J/molK]	ΔG^{mix} [kJ/mol]
Cu0	−20.03	5.61	−28.29
Cu0.25	−19.88	5.75	−28.35
Cu0.5	−19.73	5.86	−28.37
Cu0.75	−19.59	5.96	−28.37
Cu1	−19.44	6.05	−28.36
Cu1.5	−19.15	6.23	−28.32
Cu2	−18.86	6.39	−28.27

$$\Delta H^{mix} = \sum_{\substack{i=1 \\ i \neq j}}^{n} 4(\Delta H_{ij}^{mix}) c_i c_j \quad (1)$$

$$\Delta S^{conf} = -R \sum_{i=1}^{n} c_i ln c_i \quad (2)$$

$$\Delta G^{mix} = \Delta H^{mix} - T\Delta S^{conf} \quad (3)$$

where: ΔH_{ij}^{mix} is the mixing enthalpy for equiatomic composition in a binary system, c_i and c_j are the compositions of i and j elements, R is the gas constant and T analyzed temperature (in this case 1473.15 K).

It can be noticed, that the addition of copper results in the increase of configurational entropy and mixing enthalpy. The increasing value of mixing enthalpy is undesirable in the case of amorphization. Additionally, the mixing enthalpy of Cu with Fe is positive (13 kJ/mol), therefore, the phase separation should occurs in these alloys. This results with formation of crystalline phases in Cu2.0 alloy (see Fig. 1a). These phases were identified as α-Fe and Fe_2Si. To form stable amorphous phase mixing enthalpy between chemical elements should be negative and entropy as high as possible. To determine influence of these two parameters on the thermodynamics of molten alloys with different Cu content the ΔG^{mix} was calculated. It can be seen, that the changes in the value of this parameter are not linear. The lowest value of ΔG^{mix} was observed for Cu0.5 and Cu0.75 alloys and this can be associated with balance between positive influence of entropy and negative influence of mixing enthalpy from Cu addition.

To determine thermal stability and crystallization kinetics in amorphous ribbons with different Cu content DSC curves were recorded and presented in Fig. S1. It can be noticed that all alloys crystallize in two phases: α-Fe and Fe_2B. Abnormal crystallization of the first phase was observed for fragile Cu1.5 alloy. This can be associated with presence of atomic clusters in the structure, which decreases activation energy of crystallization of the first phase. To determine influence of copper content on the crystallization of second, Fe_2B phase in the Fig. 2a compared DSC curves recorded for constant heating rate equal to 10 K/min and XRD patterns (Fig. 2b) for alloys isothermal annealed at 773 K by 1 h. It can be noticed, that the shape of the first crystallization peak changes, its asymmetry increases. Additionally, with increasing copper content onset temperature of crystallization and maximum of the peak associated with crystallization of first and second phase moves towards lower values, however changes for second peak are not as visible as for first one (Table 2). Therefore, with increasing copper content increases difference ΔT between T_{x1} and T_{x2}, which is presented in Fig. 3c. These changes are associated with formation of additional Cu clusters during heating. The Cu clusters are nucleation sites of α-Fe phase, whereas boron is rejected in this process and stabilizes amorphous phase [22]. Interestingly, the changes in ΔT can be correlated with ΔG^{mix}. As can be seen in Fig. 3c, major changes of the ΔG^{mix} value cause major changes of the ΔT value, therefore the highest changes can be observed for Cu0.5 alloy, whereas with increasing addition of Cu only slightly changes of ΔT and ΔG^{mix} can be observed. These changes are important to optimize nanocrystallization process of amorphous ribbons. The lower value of T_{x1} indicates lower value of the heat treatment temperature. Additionally the higher value of ΔT indicate higher temperature range of this process. However, the negative impact of Cu content on the crystallization process can be also observed. First of all, this is important to prevent crystallization of magnetic hard Fe_xB phases, therefore ΔT should be as high as possible. However, as can be seen in Fig. 2b at the same temperature 773 K the crystallization of Fe_2B phase is different for tested alloys. For Cu0 and Cu0.25 amorphous alloy at this temperature crystallization of α-Fe still occurs (see in DSC curves) and absence of Fe_2B phase can be confirmed in XRD patterns. For the other alloys at this temperature crystallization of α-Fe stopped and the crystallization of Fe_2B phase should not started (based on the DSC curves), however this phase can be observed in the XRD patterns. This is associated with difference between isochronal and

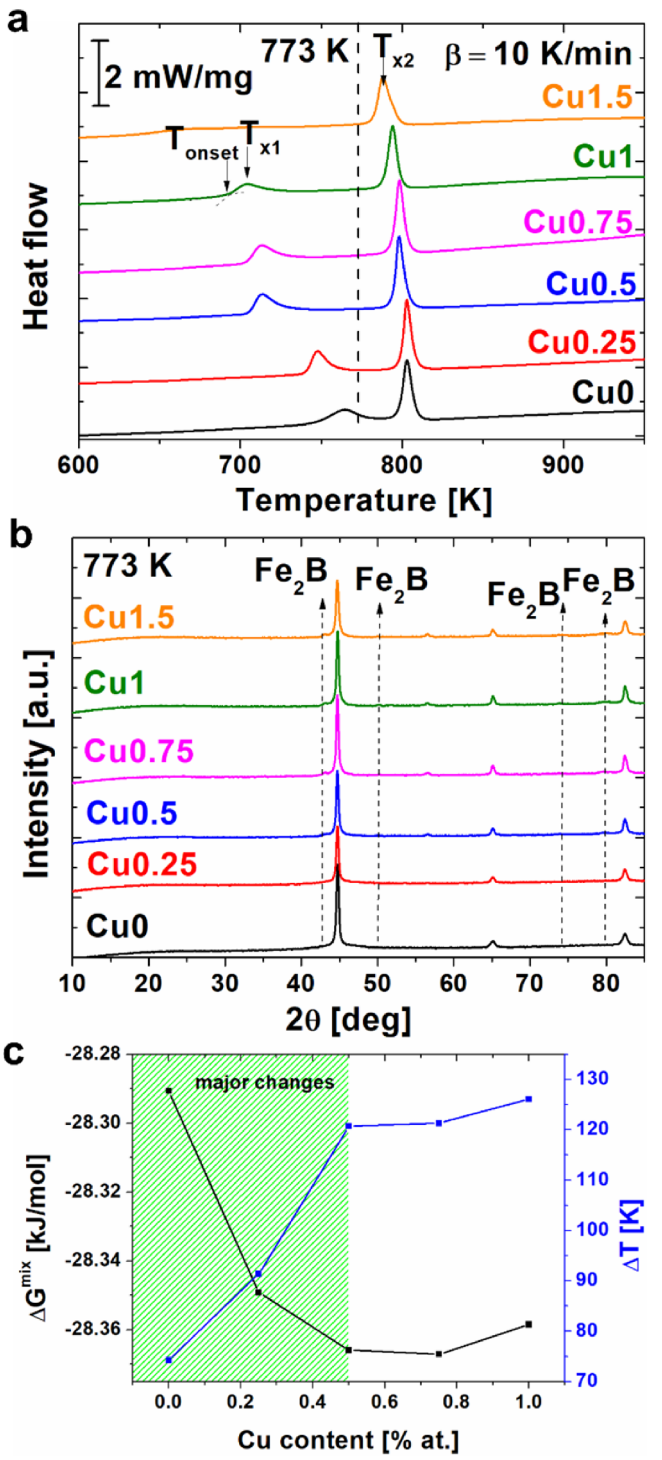

Fig. 2. a) comparison of DSC curves of alloys with different Cu content recorded at 10 K/min heating rate; b) XRD patterns of the same alloys after isothermal annealing at 773 K by 1 h with marked Fe_2B phase; c) influence of copper addition on the ΔT and $\Delta G^{mix.}$

isothermal annealing. In the case of isothermal annealing, the crystallization depends not only on the time but also on the temperature. Therefore for further optimization of the crystallization temperatures of α-Fe phase is very important to use temperatures in which crystallization of α-Fe did not stop to prevent formation of the Fe_2B phase.

The crystallization kinetics were determined for fully amorphous samples. For this purpose activation energies were calculated from Kissinger Eq. (4) for the temperature of the crystallization onset and

Table 2
The characteristic temperatures determined based on the DSC curves at 10 K/min heating rate.

Alloy	T_{onset} [K]	T_{x1} [K]	T_{x2} [K]
Cu0	728.85	744.85	803.05
Cu0.25	711.65	740.85	803.05
Cu0.5	677.45	705.35	798.15
Cu0.75	677.25	703.65	798.55
Cu1	668.05	691.35	794.15
Cu1.5	n.a.	n.a.	788.15

Table 3
The values of activation energy determined from the Kissinger plots for different characteristic temperatures.

Alloy	$E_a(onset)$ [kJ/mol]	$E_a(P1)$ [kJ/mol]	$E_a(P2)$ [kJ/mol]
Cu0	151.6	224.2	398.8
Cu0.25	210.1	210.3	419.7
Cu0.5	256.7	265.6	388.6
Cu0.75	262.4	272.0	367.8
Cu1	239.3	243.8	336.6
Cu1.5	n.a.	n.a.	338.7

maximum of the first and second peak, P1 and P2 respectively. The Kissinger plots were presented in Fig. 3a–c and the values of activation energies in Table 3.

$$\ln\left(\frac{\beta}{T^2}\right) = -\frac{E_a}{RT} + C_1 \tag{4}$$

where β is the heating rate, E_a is the activation energy, R is the gas constant, T is the temperature (temperature of crystallization onset and temperatures of different peaks) and C_1 is the constant.

It was previously reported, that the E_a calculated from the T_{onset} is associated with nucleation, whereas calculated from T_x with growth of crystalline phase. It can be noticed, that only for Cu0.25 $E_a(onset)$ is similar to $E_a(P1)$, which can be associated with presence of crystallites on the surface of ribbons. For the other alloys $E_a(P1)$ is higher than $E_a(onset)$, therefore the nucleation process is more easier than the growth of α-Fe phase. Moreover, the $E_a(onset)$ increase up to 262.4 kJ/mol for 0.75% at. Cu and then decrease to 239.3 kJ/mol for 1% at. Cu. This can be related to the increasing of entropy in these alloys, which is caused by introduction of copper. For the alloy containing 1% at. Cu the observed decreasing of the $E_a(onset)$ and $E_a(P1)$ can be associated with numerous of Cu clusters, which can be formed in amorphous matrix under continuous heating of sample.

To better understand the crystallization process the further analysis of the local activation energy was performed. According to the Ozawa-Flynn-Wall formula for isochronal crystallization, this local activation energy (E_α) can be calculated using Eq. (5):

$$\ln(\beta) = -\frac{1.052E_\alpha}{RT_\alpha} + C_2 \tag{5}$$

where T_α is a temperature corresponding to the certain crystallized fraction (α) and C_2 is the constant. The volume of the crystallized fraction can be determined as the ratio of the part area before T_α and total area of DSC peak. The α in the function of temperature for the different heating rates determined for two analyzed DSC peaks are presented in the Figs. S2 and S3. The all curves have sigmoidal shape, which is associated with nucleation and growth of the crystalline phases. Moreover, the shape of curves changes with increasing of copper addition. This is related to fast nucleation process at lower temperatures and slow growth of grains. The same tendency can be observed for the second peak. According to the Eq. (5) local activation energy was calculated for different crystallized fraction in the range of 0.1–0.9 and presented in Fig. 3d and e. It can be noticed, that the obtained values of E_α are different than these ones determined based on the Kissinger plots. The changes in the E_α are related to the nucleation and growth of crystalline phases. Generally, the local activation energy increases at the start of the crystallization process and decreases with progressive crystallization. When the E_α increases with increasing α it can be related to the existence of many tiny areas of short-range ordered atoms, such as Cu clusters. Therefore formation of nucleus is much easier than their diffusion controlled growth. The typical behavior, in which local activation energy increases at the start of the crystallization process and decreases with progressive crystallization was observed for Cu0.25, Cu0.5 and Cu0.75 alloys. For the Cu0 and Cu1

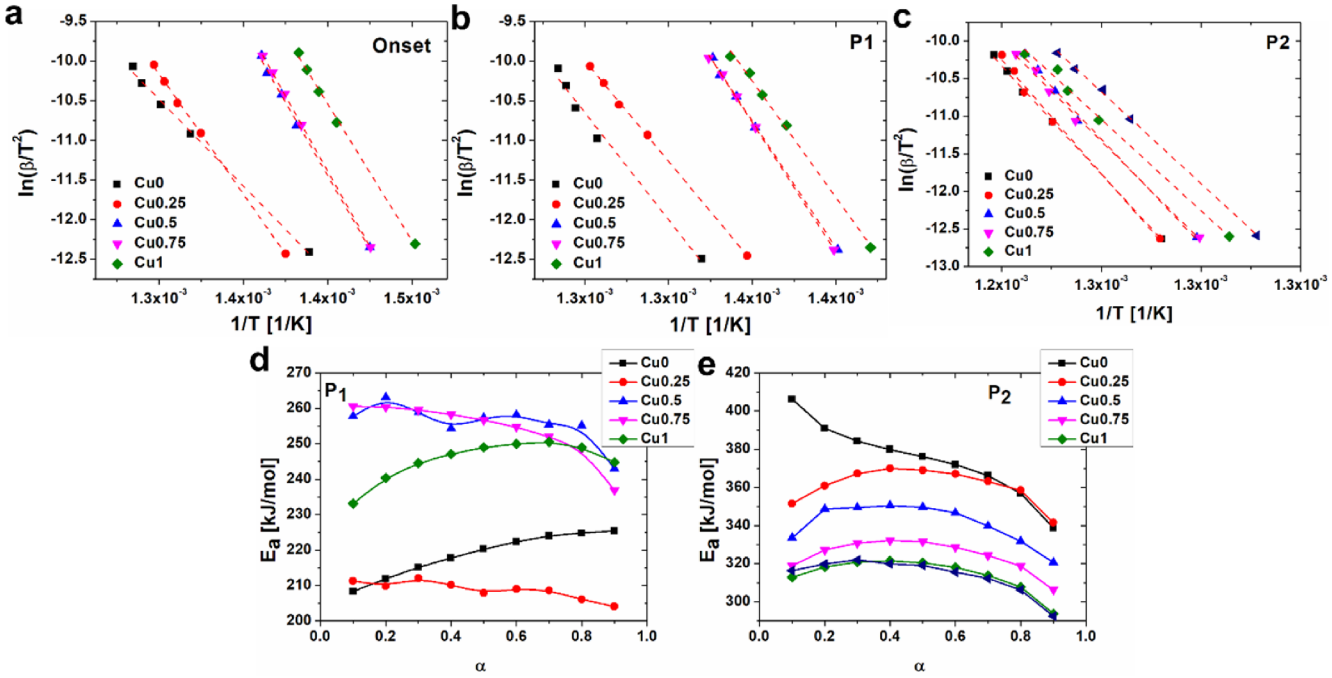

Fig. 3. a)–c) Kissinger plots for all alloys determined for crystallization onset temperatures (a) and peak temperatures (b and c); d) local activation energy of crystallization of first phase and e) local activation energy of crystallization of second phase at different crystallization fraction (α).

Table 4
The Avrami exponent calculated for 10 K/min heating rate for first (P1) and second (P2) crystallization peaks.

Alloy	n_{P1}	n_{P2}
Cu0	2.4	5.7
Cu0.25	4.8	5.6
Cu0.5	2.5	5.6
Cu0.75	2.2	3.8
Cu1	1.9	6.1
Cu1.5	n.a.	3.7

Table 5
The values of coercivity (H_c), remanence (B_r), magnetic losses (P_s) and saturation magnetization (B_{max}) at 1000 A/m determined for toroidal cores from alloys annealed in optimal condition.

Alloy	Annealing temperature [K]	H_c [A/m]	B_{max} [T]	B_r [T]	P_s [W/kg]
Cu0	658	8.87	1.59	1.02	0.45
Cu0.25	638	9.43	1.59	0.96	0.45
Cu0.5	638	9.48	1.59	0.95	0.45
Cu0.75	638	9.1	1.54	0.75	0.43
Cu1	628	10.9	1.56	0.73	0.55

alloys increasing tendency can be observed. This can be related to absence of Cu clusters (for Cu0) or with very fast nucleation process under annealing (for Cu1). Slight addition of copper decreases local activation energy of crystallization process of Fe_2B phase, especially in the nucleation stage. Moreover, with increasing Cu addition this energy decreases, which can be associated with reject of boron into amorphous matrix under crystallization of α-Fe and high ΔT, in which reordering of this boron-rich matrix should occurs.

To describe the crystallization of α-Fe and Fe_2B phases in isochronal annealing analysis of Avrami exponent (n) was performed. For the analyzed alloys average Avrami exponent was calculated according to the Augis and Bennett formula [23]:

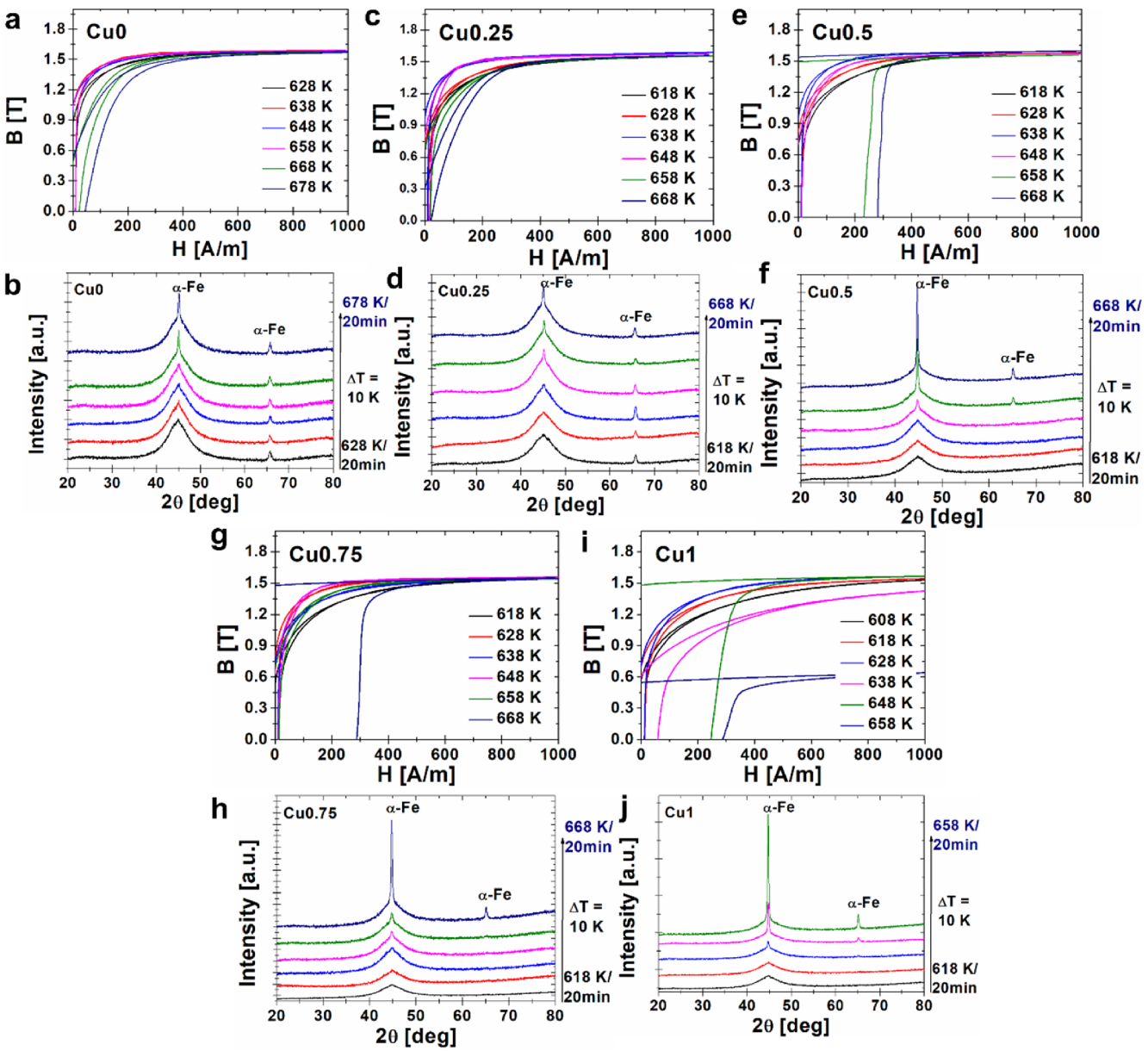

Fig. 4. Influence of annealing of cores performed from amorphous ribbons on their magnetic properties and structure: hysteresis loops (a, c, e, g, i) and corresponding XRD patterns (b, d, f, h, j) recorded for Cu0 (a, b), Cu0.25 (c, d), Cu0.5 (e, f), Cu0.75 (g, h) and Cu1 (i, j) alloys.

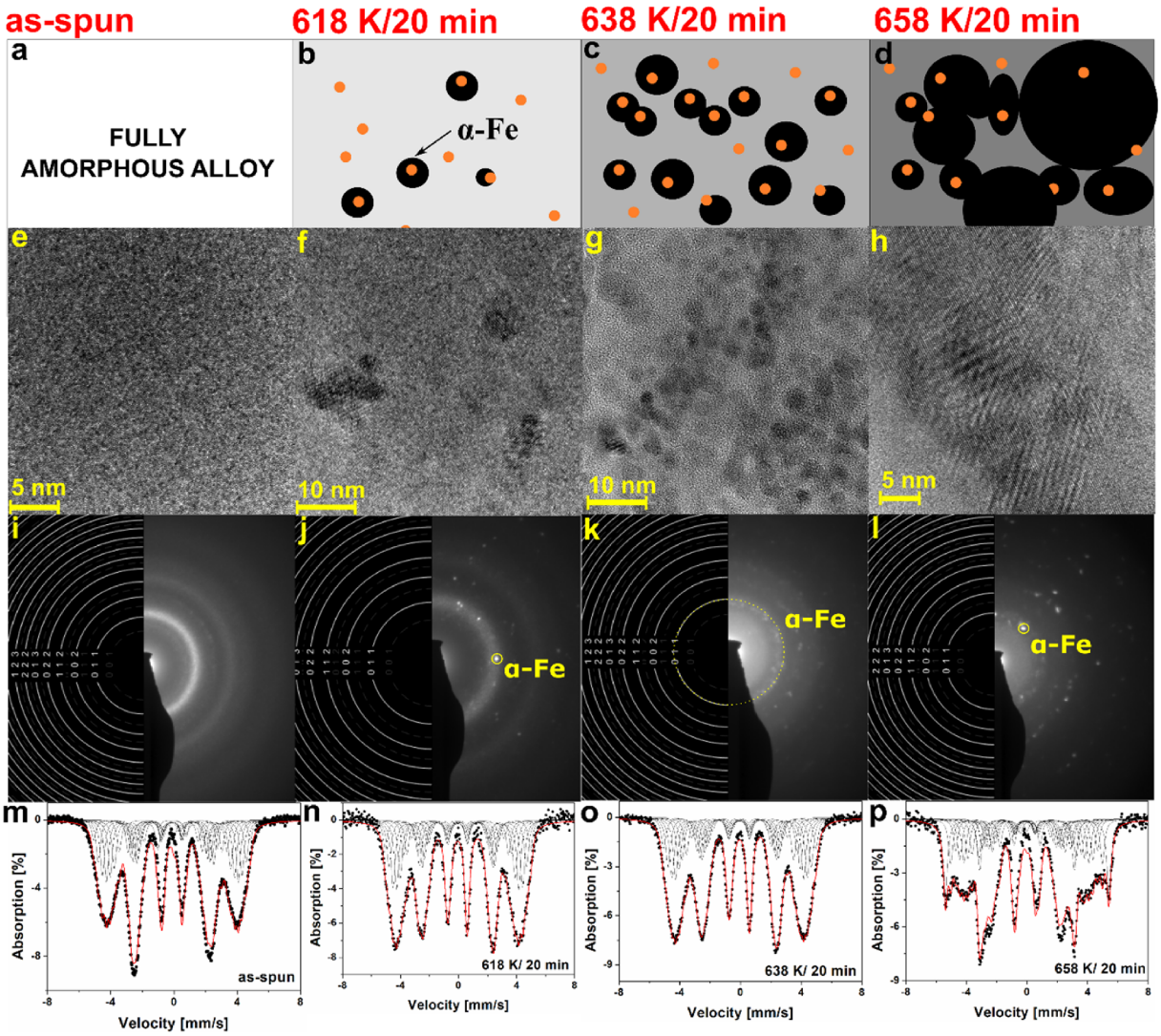

Fig. 5. Analysis of formation of nanocrystalline α-Fe phase in Cu0.5 alloy. a)–d) schematic representation of this process; e)-h) HRTEM images of Cu0.5 alloys in as-spun state (e) and after annealing by 20 min at 618 K (f), 638 K (g) and 658 K (h); i)-j) corresponding to these images SAED patterns; m)-p) Mössbauer spectra of Cu0.5 alloy in as-spun state (m) and after annealing by 20 min at 618 K (n), 638 K (o) and 658 K (p) – red lines represent the best fit.

$$n = \frac{2.5}{FWHM} \cdot \frac{T_x^2}{\frac{E_a}{R}} \tag{6}$$

where FWHM is the full width at half maximum of crystallization peak, T_x is the temperature of the maximum of crystallization peak and E_a is the activation energy determined based on the Kissinger equation. The calculated values of n for the heating rate equal to 10 K/min are listed in Table 4. It can be noticed, that only for Cu0.25 alloy crystallization of the first phase can be described by interface controlled growth with increasing nucleation rate, whereas for the other alloys by diffusion controlled growth with decreasing nucleation rate. The crystallization of the second phase can be described by interface controlled growth with increasing nucleation rate for all alloys. The results are consistent with the calculation of activation energy. The low and similar values of $E_a(onset)$ and $E_a(P1)$ for Cu0.25 are associated with existence of crystallites of α-Fe phase on the surface of ribbons, therefore the growth of other grains occurs on their surface. For the other alloys with copper at the first step of the crystallization many nucleus are formed on the Cu cluster and afterwards growth of the α-Fe phase occurs. For the Cu0 alloy the reordering of amorphous phase occurs and then nucleus are formed in amorphous matrix, therefore crystallization of this phase starts in higher temperatures. The crystallization of the Fe_2B phase is more difficult, because the existence of α-Fe phase grains blocks the diffusion process and the growth of this phase is possible only on the α-Fe phase grain boundaries [24]. Therefore, the local activation energy of formation of new nucleus increases with increasing crystallization fraction up to α = 0.4 and then decrease, which is associated with growth of this phase. Only for Cu0 alloy this energy decreases with increasing crystallization fraction and is very high at the start of crystallization process. It is very difficult to form nucleus of Fe_2B phase, whereas their growth is much easier. This can easily explain why on the XRD patterns of annealed at 773 K alloys the Fe_2B phase occurs for alloys with higher addition of Cu, whereas its absence was observed for Cu0 alloy.

To prepare soft magnetic materials isothermal annealing of amorphous, toroidal cores was performed in vacuum in different temperatures by 20 min. On the basis of analysis of hysteresis loops and XRD patterns the optimum parameters of heat treatment were chosen for all alloys with different Cu addition. The obtained results are presented in Fig. 4. It can be noticed, that the different temperatures for alloys with different Cu content must be used to obtain cores with low coercivity (H_c) and high saturation magnetization (B_{max}). The values of magnetic parameters such as coercivity, remanence (B_r), power core losses (P_s) and saturation magnetization at 1000 A/m for all cores are presented in

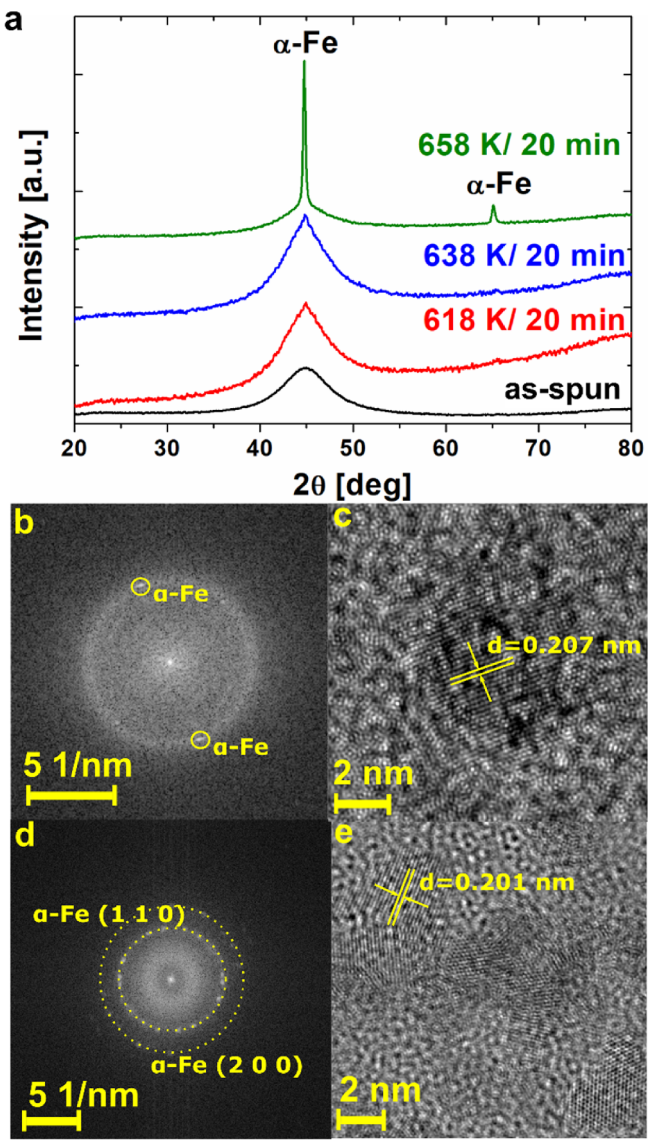

Fig. 6. a) XRD patterns of Cu0.5 alloy in as-spun state and after annealing by 20 min at different temperatures; b) FFT from area presented on (c) with marked diffused reflexes corresponding to the oriented α-Fe crystallites; c) HRTEM image of nanocrystalline α-Fe with marked distance between (1 1 0) lattice planes; d) FFT form area presented on (e) with marked diffraction rings corresponding to the randomly oriented α-Fe crystallites; e) HRTEM image of nanocrystalline α-Fe with marked distance between (1 1 0) lattice planes;

Table S1, whereas in Table 5 presented the same parameters for the materials with the best soft magnetic properties. As can be seen, with increasing Cu addition the lower annealing temperature is needed to obtain alloys with low coercivity. With increasing temperature of annealing the growth of α-Fe crystallites occurs and power core losses and coercivity increase. The best magnetic parameters can be obtained for materials in which coexistence of amorphous phase and nanocrystallites was confirmed (see XRD patterns in Fig. 4.). In the highest temperatures coercivity and power core losses increase significantly, which is associated with growth of α-Fe crystallites (Fig. 5b, d, f, h and j). Interestingly, alloy without Cu is characterized also by good magnetic parameters, however high temperature of heat treatment is required and growth of α-Fe cannot be easily controlled.

For better understanding the formation process of the α-Fe nanocrystallites and the influence of heat treatment temperature on the magnetic properties analysis of HRTEM images, SAED patterns, Mössbauer spectra and XRD patterns of Cu0.5 alloy was performed. Obtained results are presented in Figs. 5 and 6. Presented in Fig. 6a XRD patterns confirm, that the annealing of amorphous alloy results in formation of local ordered regions in amorphous matrix for low heat treatment temperature. The usage of higher temperature (658 K) results in formation of much bigger crystallites. On the basis of performed analysis the schematic representation of this process was proposed (Fig. 5a–d). The HRTEM image (Fig. 5e) as well as SAED pattern (Fig. 5i) and Mössbauer spectrum (Fig. 5m) confirm, that the melt spun Cu0.5 alloy is fully amorphous. The disordered structure can be observed on the HRTEM image and broad diffraction rings on SAED pattern. Moreover, Mössbauer spectrum shows six broadened lines, characteristic for amorphous ferromagnetic alloys [25]. After annealing at 618 K by 20 min in amorphous matrix nanocrystallites are formed (Fig. 5f). These crystallites are associated with reorganization of amorphous structure and formation of α-Fe phase, which was confirmed by analysis of SAED pattern (Fig. 5j) and analysis of the crystallites structure (Fig. 6b and c). The distance between (1 1 0) lattice planes in α-Fe phase was identified and marked in Fig. 6b. The Mössbauer spectra of Cu0.5 alloy annealed at 618 K and 638 K confirm the reorganization of amorphous structure, which is associated with α-Fe phase crystallization. The values of B_{hf} presented in Table S1 are connected with Fe atoms surrounded mainly by boron and silicon atoms. The values of B_{hf} close to 24 T and 18 T are connected with iron which has about two and four, respectively, boron atoms as the nearest neighbors. It can be noticed, that the B_{hf} = 15.1 T disappears and others increase, which can be associated with crystallization of iron and silicon into α-Fe phase (Fig. 5n and o, Table S1). A small increase in the values of hyperfine magnetic field for these samples can be related to enhanced magnetic interaction caused by nanocrystallization process. Moreover, the broad lines confirms the segregation process. These results are confirmed by SAED pattern (Fig. 5k) and by analysis of HRTEM images (Figs. 5g and 6d, e) recorded for Cu0.5 alloy annealed at 638 K. The observed structure is responsible for good soft magnetic properties of alloy. Figs. 5g and 6e presents, that the nanocrystallites of α-Fe phase are embedded in amorphous matrix. This composite structure results in the highest soft magnetic properties, which is associated with the obtained balance between positive and negative magnetostriction [22]. The usage of higher temperature (658 K) results in the growth of nanocrystalites and formation of polycrystalline alloy with high coercivity (231 A/m) and high power core losses (9.6 W/kg). The Mössbauer spectrum of this alloy (Fig. 5p) confirms phase segregation. The observed lines are narrower, which is associated with formation of locally ordered atomic structure in the alloy. The formation of new phases, such as Fe-Co, Fe-B results in formation of areas rich in others chemical elements and hence lower B_{hf} = 15. T (Table S1).

4. Conclusions

The crystallization process of $Fe_{79.8-x}Co_2Cu_xMo_{0.2}Si_4B_{14}$ (x = 0, 0.25, 0.5, 0.75, 1, 1.5, 2) amorphous alloys was described. It was confirmed, that the amorphous ribbons can be prepared from alloys with Cu addition below 2 at. % and flexible ribbons from alloys with Cu addition below 1 at.%. Therefore, it was possible to prepare toroidal cores from 5 alloys with Cu addition in the range of 0–1 at. %. The double stage crystallization of amorphous samples studied by DSC technique and X-ray diffraction method is associated with diffusion controlled growth with decreasing nucleation rate of α-Fe phase and interface controlled growth with increasing nucleation rate of Fe_2B phase. The crystallization of second phase is more difficult. This is associated with grains of nanocrystalline α-Fe phase, which block the diffusion process. Therefore Fe_2B phase crystallize on the grain boundaries of α-Fe phase. It can be concluded, that the higher value of ΔT indicate the easier formation of Fe_2B phase nucleus than their growth, which in turn can be related to the time needed for reorganization of remaining boron rich amorphous phase. The controlled nucleation and α-Fe phase growth allow to prepare soft magnetic

material with high saturation magnetization about 1.6 T, low coercivity (~9 A/m) and very low power core losses (about 0.45 W/kg). This is associated with formation of composite structure, in which nanometric α-Fe crystallites are distributed in boron rich amorphous matrix. However, the determination of the optimal parameters of heat treatment is very important to avoid uncontrolled growth, which manifests in increase of coercivity even to 288 A/m. On the other hand, too low temperature of heat treatment results only in the reorganization of amorphous matrix, formation of Cu clusters and precipitation of low amount of α-Fe nanocrystallites.

Acknowledgments

This work was co-financed by the National Centre for Research and Development Grant TECHMATSTRATEG No. 1/347200/11/NCBR/2017, the internal source: IMN own studies, IMN project report no. 7773/18 and by the European Union Operational Programme Smart Growth, through the Grant of Regional Agenda for Science and Research (POIR.04.01.02-00-0001/16).

Appendix A. Supplementary data

Supplementary data to this article can be found online at https://doi.org/10.1016/j.jmmm.2019.165951.

References

[1] T. Gheiratmand, H.R.M. Hosseini, Finemet nanocrystalline soft magnetic alloy: investigation of glass forming ability, crystallization mechanism, production techniques, magnetic softness and the effect of replacing the main constituents by other elements, J. Magn. Magn. Mater. 408 (2016) 177–192, https://doi.org/10.1016/j.jmmm.2016.02.057.

[2] K. Takenaka, A.D. Setyawan, P. Sharma, N. Nishiyama, A. Makino, Industrialization of nanocrystalline Fe-Si-B-P-Cu alloys for high magnetic flux density cores, J. Magn. Magn. Mater. 401 (2016) 479–483, https://doi.org/10.1016/j.jmmm.2015.10.091.

[3] J. Xu, Y. Yang, W. Li, Z. Xie, X. Chen, Effect of Si addition on crystallization behavior, thermal ability and magnetic properties in high Fe content Fe-Si-B-P-Cu-C alloy, Mater. Res. Bull. 97 (2018) 452–456, https://doi.org/10.1016/j.materresbull.2017.09.042.

[4] M. Nabiałek, Soft magnetic and microstructural investigation in Fe-based amorphous alloy, J. Alloys Compd. 642 (2015) 98–103, https://doi.org/10.1016/j.jallcom.2015.03.250.

[5] C. Wang, A. He, A. Wang, J. Pang, X. Liang, Q. Li, C. Chang, K. Qiu, X. Wang, Effect of P on glass forming ability, magnetic properties and oxidation behavior of FeSiBP amorphous alloys, Intermetallics 84 (2017) 142–147, https://doi.org/10.1016/j.intermet.2016.12.024.

[6] C.C. Cao, Y.G. Wang, L. Zhu, Y. Meng, Y.D. Dai, J.K. Chen, Evolution of structural and magnetic properties of the FeCuBP amorphous alloy during annealing, J. Alloys Compd. 722 (2017) 394–399, https://doi.org/10.1016/j.jallcom.2017.06.147.

[7] J.A. Moya, Improving soft magnetic properties in FINEMET-like alloys. A study, J. Alloys Compd. 622 (2015) 635–639, https://doi.org/10.1016/j.jallcom.2014.10.124.

[8] X.D. Fan, B.L. Shen, Crystallization behavior and magnetic properties in High Fe content FeBCSiCu alloy system, J. Magn. Magn. Mater. 385 (2015) 277–281, https://doi.org/10.1016/j.jmmm.2015.03.033.

[9] W. Li, Y.Z. Yang, J. Xu, C.X. Xie, Glass formation and magnetic properties of Fe–Hf–Zr–M (M = metalloids Si, P, and B and metal Al) high-iron alloys, J. Alloys Compd. 710 (2017) 644–649, https://doi.org/10.1016/j.jallcom.2017.03.315.

[10] X. Li, J. Liu, C. Qu, K. Song, L. Wang, Effects of Nb on the precipitation of α-Fe, glass forming ability and magnetic properties of $Fe_{85}B_{10}P_5$ alloys, J. Alloys Compd. 694 (2017) 643–646, https://doi.org/10.1016/j.jallcom.2016.09.298.

[11] R. Nowosielski, M. Kadziołka-Gaweł, P. Gebara, D. Szyba, R. Babilas, Magnetic properties and structure after crystallization of $Fe_{80-x}B_{20}Nb_x$ (x = 4, 6, 10) metallic glasses, Acta Phys. Pol. A 131 (2017), https://doi.org/10.12693/APhysPolA.131.1212.

[12] J. Dai, Y.G. Wang, L. Yang, G.T. Xia, Q.S. Zeng, H.B. Lou, Thermal dependence of structural and magnetic properties in an amorphous Fe-Si-B-Cu alloy, J. Alloys Compd. 695 (2017) 1266–1270, https://doi.org/10.1016/j.jallcom.2016.10.255.

[13] P. Gupt, A. Gupta, A. Shukl, T. Ganguli, A.K. Sinha, G. Principi, A. Maddalena, Structural evolution and the kinetics of Cu clustering in the amorphous phase of Fe-Cu-Nb-Si-B alloy, J. Appl. Phys. 110 (2011), https://doi.org/10.1063/1.3622325.

[14] T. Ohkubo, H. Kai, D.H. Ping, K. Hono, Y. Hirotsu, Mechanism of heterogeneous nucleation of α-Fe nanocrystals from $Fe_{89}Zr_7B_3Cu_1$ amorphous alloy, Scr. Mater. 44 (2001) 971–976, https://doi.org/10.1016/S1359-6462(00)00689-8.

[15] K.G. Pradeep, G. Herzer, P. Choi, D. Raabe, Atom probe tomography study of ultrahigh nanocrystallization rates in FeSiNbBCu soft magnetic amorphous alloys on rapid annealing, Acta Mater. 68 (2014) 295–309, https://doi.org/10.1016/j.actamat.2014.01.031.

[16] Y.M. Chen, T. Ohkubo, M. Ohta, Y. Yoshizawa, K. Hono, Three-dimensional atom probe study of Fe-B-based nanocrystalline soft magnetic materials, Acta Mater. 57 (2009) 4463–4472, https://doi.org/10.1016/j.actamat.2009.06.008.

[17] K. Hono, D.H. Ping, M. Ohnuma, H. Onodera, Cu clustering and Si partitioning in the early crystallization stage of an $Fe_{73.5}Si_{13.5}B_9Nb_3Cu_1$ amorphous alloy, Acta Mater. (1999), https://doi.org/10.1016/S1359-6454(98)00392-9.

[18] T. Bitoh, A. Makino, A. Inoue, T. Masumoto, Random anisotropy model for nanocrystalline soft magnetic alloys with grain-size distribution, Mater. Trans. 44 (2003) 2011–2019, https://doi.org/10.2320/matertrans.44.2011.

[19] H.R. Lashgari, D. Chu, S. Xie, H. Sun, M. Ferry, S. Li, Composition dependence of the microstructure and soft magnetic properties of Fe-based amorphous/nanocrystalline alloys: a review study, J. Non. Cryst. Solids 391 (2014) 61–82, https://doi.org/10.1016/j.jnoncrysol.2014.03.010.

[20] M. Klinger, More features, more tools, more CrysTBox, J. Appl. Crystallogr. 50 (2017) 1226–1234, https://doi.org/10.1107/S1600576717006793.

[21] M. Klinger, A. Jäger, Crystallographic Tool Box (CrysTBox): automated tools for transmission electron microscopists and crystallographers, J. Appl. Crystallogr. 48 (2015) 2012–2018, https://doi.org/10.1107/S1600576715017252.

[22] R.K. Nutor, X. Fan, S. Ren, M. Chen, Y. Fang, Research progress of stress-induced magnetic anisotropy in Fe-based amorphous and nanocrystalline alloys, J. Electromagn. Anal. Appl. 09 (2017) 53–72, https://doi.org/10.4236/jemaa.2017.94006.

[23] J.A. Augis, J.E. Bennett, Calculation of the Avrami parameters for heterogeneous solid state reactions using a modification of the Kissinger method, J. Therm. Anal. (1978), https://doi.org/10.1007/BF01912301.

[24] K. Chrissafis, M.I. Maragakis, K.G. Efthimiadis, E.K. Polychroniadis, Detailed study of the crystallization behaviour of the metallic glass Fe75Si9B16, J. Alloys Compd. (2005), https://doi.org/10.1016/j.jallcom.2004.05.062.

[25] H. Oukris, H. Lassri, E.H. Sayouty, J.M. Greneche, Magnetic and Mössbauer studies of amorphous Fe-Al-Er-B ribbons, J. Magn. Magn. Mater. 260 (2003) 23–27, https://doi.org/10.1016/S0304-8853(02)00059-8.